JPSE (Journal of Physical Science and Engineering), Vol. 7, No. 2, 2022, Page 108–115.
DOI: 10.17977/um024v7i22022p108

JPSE
(Journal of Physical Science and Engineering)

http://journal2.um.ac.id/index.php/jpse
EISSN: 2541-2485

Oxygen Gas Vacuum Plasma Treatment on PVA/Chitosan/ HAp Scaffold Nanofiber

Received
01 September 2022

Revised
14 October 2022

Accepted for Publication
01 November 2022

Published
30 December 2022

Hartatiek[1,2], N Shofura[1], M I Wuriantika[1], Yudyanto[1,2], M Nurhuda[2], Masruroh[2*], D J D H Santjojo[2], and N Ahmad[3]

1. Department of Physics, Faculty of Mathematics and Natural Sciences, Universitas Negeri Malang, Jl. Semarang 5, Malang, 65145, Indonesia.
2. Department of Physics, Faculty of Mathematics and Natural Sciences, Universitas Brawijaya, Jl. Veteran, Malang, 65145, Indonesia.
3. Department School of Mechanical Engineering, Faculty of Engineering, Universiti Teknologi Malaysia, Johor, 81310, Malaysia.

***E-mail:** ruroh@ub.ac.id

Abstract
Scaffold in the form of nanofibers in bone tissue engineering applications continues to be developed. In this study, nanofibers are composed of PVA/CS/HAp with characteristics that can support medical applications such as bone tissue engineering. Vacuum plasma treatment was carried out to modify the nanofiber surface. The results of the morphological analysis showed that the vacuum plasma treatment of oxygen gas caused the surface of the PVA/CS/HAp nanofibers to become rougher with a change in diameter. Before the oxygen gas vacuum plasma treatment, the diameter of the nanofiber had a range of 83–365 nm. After the oxygen gas vacuum plasma treatment, the diameter had a size range of 105–293 nm. Furthermore, the vacuum plasma treatment carried out showed increased hydrophilic properties. The average contact angle values before and after oxygen gas vacuum plasma treatment were (39.0 ± 0.0005)° and (10.3 ± 0.0005)°, respectively.
Keywords: Vacuum plasma, nanofiber, morphology, hydrophilic.

1. Introduction

Biomedical technology is being developed in terms of bone tissue engineering to repair damaged bones [1], [2]. In order to optimize tissue regeneration, the development of tissue engineering products in the form of scaffolds is continuously being carried out [3]. The characteristics of the scaffold can be influenced by the material used. Hydroxyapatite (HAp) is one of the suitable biomaterials as a scaffold material because it is bioactive and biocompatible with bone tissue [4]. In addition, studies of HAp have not shown inflammatory response, pyrogenetic, and toxicity [5], [6]. HAp can be used to replace damaged bone tissue due to bone abnormalities, fractures, cancer, and others. However, HAp has the disadvantage of high fragility [7].

Therefore, it is necessary to add a polymer to reduce this weakness. The natural polymer that is suitable for combining with HAp is Chitosan (CS). CS has been widely developed for drug formulations because it is non-toxic, biocompatible, bioactive, and biodegradable [8]. In addition to CS, Polyvynil Alcohol (PVA) was chosen in this study. The selection of PVA is based on the nature of this material, which is non-toxic, hydrophilic, biocompatible, and biodegradable. Besides that, PVA has the ability to form fibers when electrospinning [9]–[11].

In tissue engineering, scaffolds must have hydrophilic properties to support and avoid failure during implantation. One way to increase the hydrophilic properties of nanofibers is to modify the surface of the nanofibers using vacuum plasma treatment. Plasma treatment is suitable for surface modification without changing the material's properties [12], [13]. In this study, a plasma technique was used by firing oxygen on the surface of the scaffold so that plasma ions were excited [14]. Oxygen gas was chosen because oxygen ions are quite reactive on the surface of the PVA/CS/HAp nanofibers to produce changes on their surface without any side effects on their physical structure [15]. Research on PVA/CS/HAp with modified oxygen gas vacuum plasma has yet to be widely reported. In this study, vacuum plasma treatment on PVA/CS/HAp nanofibers will be studied further, especially on the surface

morphology and hydrophilic properties, which significantly influence bone tissue engineering applications.

2. Method

2.1. Synthesis of HAp

The synthesis of HAp was initiated by dissolving as much $Ca(OH)_2$ into HNO_3 to obtain a solution of $Ca(NO_3).2H_2O$ using a magnetic stirrer at a speed of 400 rpm and temperature of 30 °C for 30 minutes. Dropped with $Ca(NO_3).2H_2O$ solution on the solution of $(NH4)_2HPO_4$. After that, drop in NH_4OH until the pH of the solution reaches 9–10. The chemical reaction for synthesis HAp showed in Equation 1.

$$10Ca_{10}(NO_3)_2.2H_2O_{(aq)} + 6(NH_4)_2HPO_{4(aq)} + 8NH_4OH_{(aq)} \rightarrow Ca_{10}(PO_4)_6(OH)_{2(s)} + 20NH_4NO_{3(aq)} + 46H_2O_{(l)} \quad (1)$$

The solution was deposited for 12 hours. The precipitate was washed using DI water until the pH reached 7–8, filtered using fine filter paper, and then sonicated for 30 minutes. All samples were dried at 100 °C for one hour, so H_2O levels disappeared. The sample is ready to be XRD characterized to determine the purity of the phase, crystal grain size, and crystallinity. SEM EDX to determine the structure and Ca/P ratio of the sample.

2.2. Synthesis of PVA/CS/HAp Nanofiber

Dissolve 8% and 20% HAp in 5 ml of aquades was then stirred at a speed of 700 rpm and room temperature for 30 minutes. The volume of the 5 mL PVA/CS polymer solution that had been prepared was reduced by 0.5 mL and then stirred at a speed of 700 rpm at 130 °C for 2 hours until it was homogeneous. The solution was sonicated for 60 minutes. After that, the solution was an electrospinning voltage of 12 kV and a flow rate of 50 µL/minute for 30 minutes. Make initial observations using an optical microscope to see the formation of nanofibers. Treatment of plasma vacuum of oxygen gas pressure is set to 30 Pascal, voltage to 100 kV. FTIR and SEM then characterized the PVA/CS/HAp composites. Figure 1 shows the synthesis procedure of PVA/CS/HAp nanofiber.

2.3. Characterizations

The characterization instrument used in this study was X-Ray Diffraction (XRD) brand PANalytical type X'Pert Pro which was used to determine the crystal phase, crystallite size, and lattice parameters. The Shimadzu brand FTIR characterization was carried out to determine the functional groups and compounds contained in the sample. The morphology of PVA/CS/HAp nanofibers before and after treatment was characterized by SEM brand FEI (Inspect S50). The hydrophilic properties of PVA/CS/HAp nanofiber were measured by measuring the contact angle of the water droplets as much as 15 µL above the sample surface.

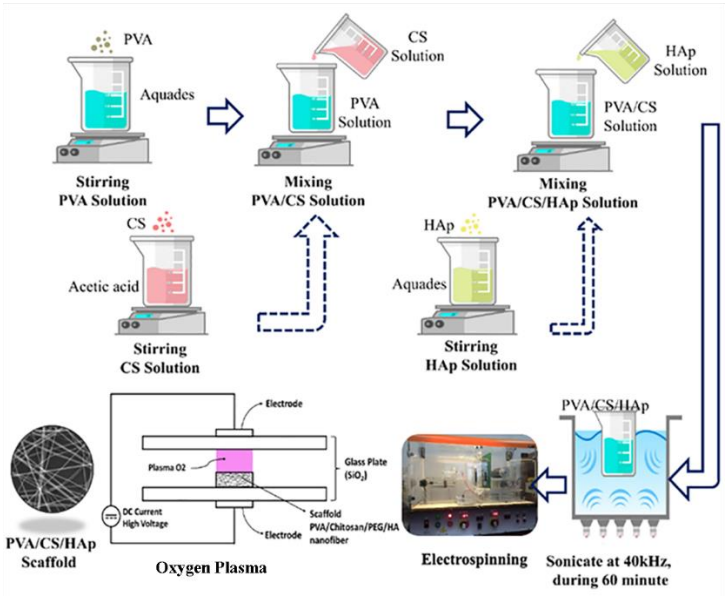

Figure 1. Synthesis of PVA/CS/HAp nanofiber.

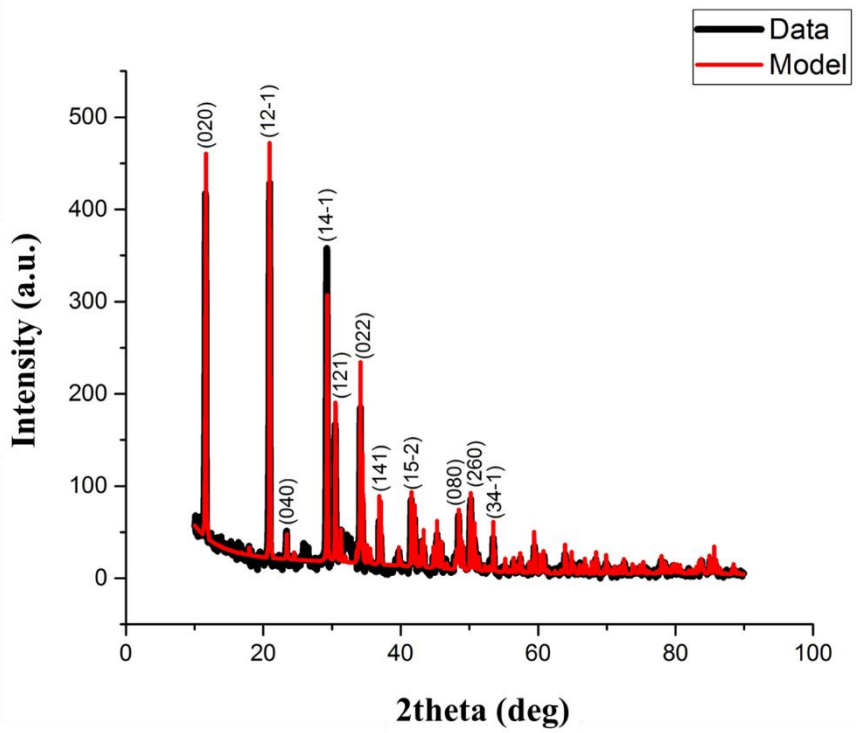

Figure 2. XRD pattern of HAp nanoparticles.

3. Result and Discussion

3.1. XRD Studies of HAp Nanoparticle

Figure 2 shows the XRD diffraction pattern of HAp. The synthesis of HAp by coprecipitation for 12 hours resulted in the Brushite phase. The synthesis method was coprecipitation with a deposition time of 12 hours. Based on the XRD results, Brushite peak characteristics were detected in the sample. Brushite is a phosphate mineral found in bones and teeth with the chemical formula $CaHPO_4.2H_2O$ [16]. The influence of an inappropriate pH can cause the presence of the brushite phase during synthesis. Previous studies have shown that synthesizing calcium phosphate with a pH > 7 will produce HAp, while at pH < 7 can produce brushite [17].

The results show the Brushite phase has lattice parameters a = 5.819 Å, b = 15.1816 Å, c = 6.2496 Å, $\alpha = \gamma = 90°$, and $\beta = 25.78°$ with a monoclinic crystal structure and group space I1A1 and the crystallite size was 39.15 nm. In addition, the degree of crystallinity in this study is calculated using Equation 2.

$$\chi_c = \frac{\text{Area Fraction of Crystal}}{\text{Area Fraction of Crystal + Area Fraction of Amorf}} \times 100\% \quad (2)$$

The calculation using Equation 2 shows that the degree of crystallinity results is 44.80%. This value fulfills the crystallinity level that must be met in the body, around 40–60%. ISO standardized specifications (ISO 13779-1: 2000) state that to make HAp coatings that have sufficient mechanical strength, at least they must have a degree of crystallinity of more than 45%.

3.2. Morphology of HAp Nanoparticles

The synthesis of HAp using the coprecipitation method in this study produced HAp in the form of partially agglomerated nanoparticles. The occurrence of agglomeration can occur due to van der Waals forces, which has a significant effect because it has an extensive surface area to volume ratio. It causes the nanoparticles to agglomerate to get the particles in a stable state [18]. Morphological analysis of HAp using SEM-EDX, as shown in Figure 3a. The average diameter of HAp is 46.8 ± 11.11 nm with a diameter distribution of 26.9–74.4 nm, porosity is 77%, and Ca/P ratio is 1.49 (Figure 3b). The Ca/P ratio of HAp is 1.49. This result is lower than the theoretical Ca/P ratio of 1.67 [19], [20].

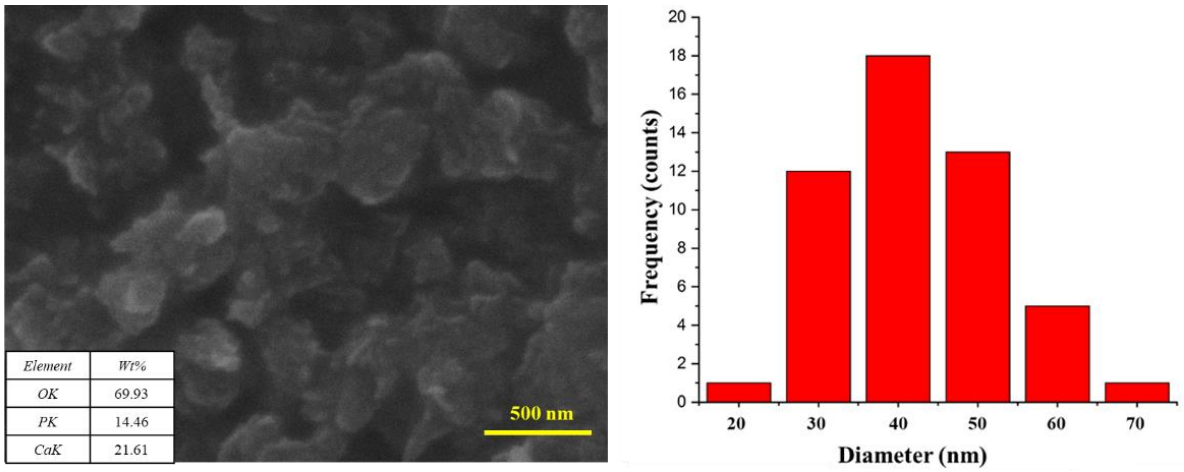

Figure 3. (a) Morphology and (b) diameter distribution of HAp nanoparticles.

3.3. FTIR Analysis of PVA/CS/HAp Nanofiber

From the results of the FTIR spectra in Figure 4, the characteristics of the functional groups of PVA, CS, and HAp in the nanofibers can be seen, where the PVA functional groups are CH, CO, and OH [21], [22]. The CS functional groups are NH and CH [23], and the HAp functional groups are OH, CO_3, and PO_4 [24]. The primary PVA spectrum can be observed in the C-H alkyl stretching band (2908 cm^{-1}) and the hydroxyl band for pure alcohol that occurs in the unbonded –OH stretching (3343 cm^{-1}). The absorption band C-O stretching occurs at a wave number of 1097 cm^{-1} due to the crystallinity of PVA [21], [22]. The spectrum of chitosan can be confirmed by the presence of peaks showing amino bonds at 1433 cm^{-1} (CH bending) and amide bonds at 3343 cm^{-1} (NH). Both groups were obtained from the N-deacety-lation bond in chitin [23]–[25].

Based on the XRD results showing the formation of a brushite phase, previous studies reported that the HAp and brushite functional groups occur at the same wavelength [26], [27]. The presence of brushite and HAp in this study was confirmed by the stretching functional group CO_3^{2-} (v3) at wave number 1433 cm^{-1} replacing –OH in the HAp lattice and CO_3^{2-} (v2) at a wave number of 856 cm^{-1} replacing PO_4^{-3}. If both functional groups appear, it can be said that the sample is almost the same as the mineral in bone [28]. The band at a wave number of 581 cm^{-1} is due to the bending bond of PO_4^{-3} while the band at a wave number of 1092 cm^{-1} is due to the stretching bond of PO_4^{-3} [29].

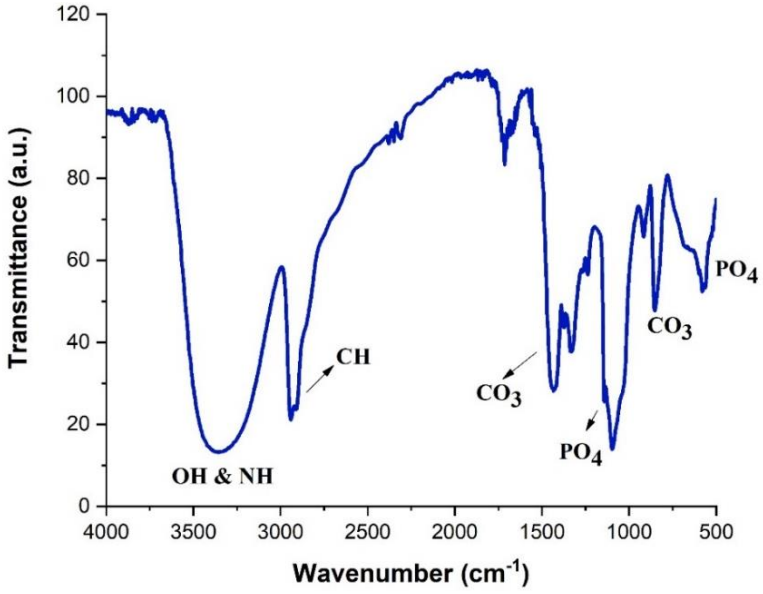

Figure 4. FTIR spectrum of PVA/CS/HAp nanofiber.

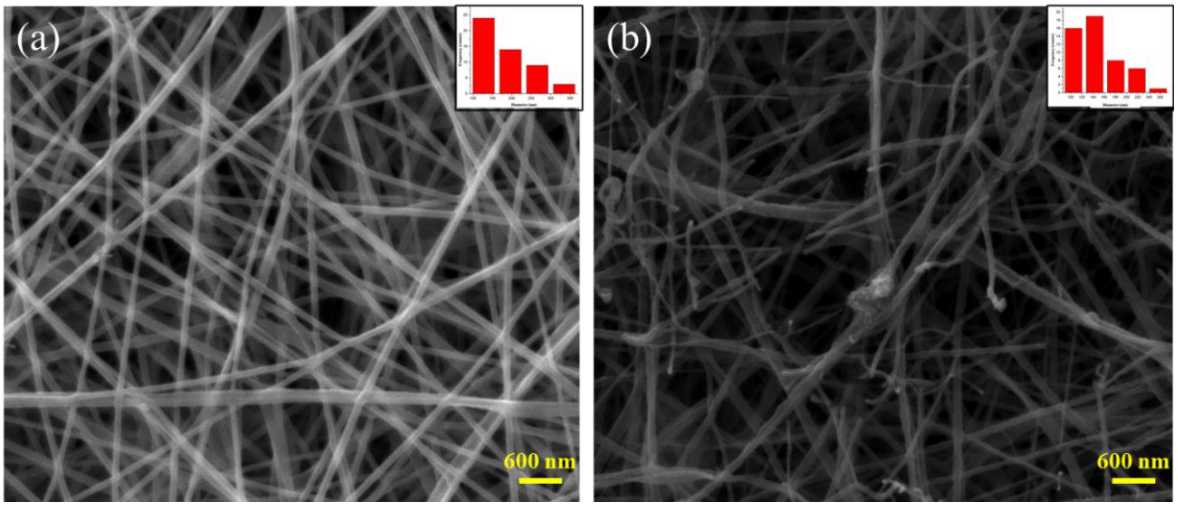

(a) (b)

Figure 5. Morphology of PVA/CS/HAp nanofiber (a) before treatment, and (b) after treatment.

3.4. Morphology of PVA/CS/HAp Nanofiber

Morphology before and after oxygen gas vacuum plasma treatment of PVA/CS/HAp nanofibers was analyzed using SEM. Oxygen gas vacuum plasma treatment is carried out to modify the surface of the scaffold PVA/CS/HAp nanofibers. It can be seen in Figure 5, PVA/CS/HAp nanofibers before and after oxygen gas vacuum plasma treatment, the morphology of the nanofibers looked different.

The surface morphology of the PVA/CS/HAp nanofibers Figure 5a appears smoother with a uniform diameter. Furthermore, in Figure 5b, nanofiber changes in diameter size and surface morphology become rougher because of the broken fiber. That occurs because the oxygen gas vacuum plasma treatment is quite reactive on the surface of the PVA/CS/HAp nanofibers, causing changes to the surface [15]. In medical applications, the diameter of nanofiber scaffolds is in the range of 50–500 nm [30]. In this study, the diameter of the nanofibers before treatment was in the range of 83–365 nm, while after the Oxygen gas vacuum plasma treatment, the diameter of the nanofibers was in the range of 105–293 nm, so both were in the nanofiber scaffold size range for medical applications such as bone tissue engineering.

3.5. Hydrophilic Properties of PVA/CS/HAp Nanofiber

The hydrophilic properties of the nanofiber can be determined by measuring the contact angle. If the contact angle is $< 90°$, the sample can be said to have hydrophilic properties. Otherwise, if $> 90°$, the sample has hydrophobic properties. This study conducted the contact angle test on PVA/CS/HAp nanofibers before and after oxygen gas vacuum plasma treatment. Oxygen gas vacuum plasma treatment was carried out for two periods, 2 and 4 minutes. The results are presented in Table 1.

The measurement of the contact angle showed that the duration of the oxygen gas vacuum plasma treatment increased the hydrophilic properties of the sample. The surface roughness of the sample can cause an increase in the hydrophilic nature of this sample. As in the SEM results (Figure 5), the surface morphology of the PVA/CS/HAp nanofibers became rougher after oxygen gas vacuum plasma treatment was carried out. These results are in accordance with previously reported research that vacuum plasma treatment can increase the hydrophilicity of a sample due to the influence of surface morphology which becomes rougher [31], [32].

Table 1. Contact angle values of PVA/CS/HAp nanofibers.

Treatment	Right Angle	Left Angle	Average
Non-Treatment	(38.6 ± 0.0005)°	(39.5 ± 0.0005)°	(39.0 ± 0.0005)°
2 minutes	(19.8 ± 0.0005)°	(19.9 ± 0.0005)°	(19.8 ± 0.0005)°
4 minutes	(10.2 ± 0.0005)°	(10.5 ± 0.0005)°	(10.3 ± 0.0005)°

4. Conclusion

HAp based on minerals from limestone synthesized by the coprecipitation method shows the brushite phase ($CaHPO_4.2H_2O$) with a monoclinic crystal structure having a crystal size of 39.15 nm with a Ca/P ratio of 1.49. The influence of an inappropriate pH can cause the presence of the brushite phase during synthesis. Oxygen gas vacuum plasma treatment carried out on PVA/CS/HAp nanofibers affects the surface morphology of the composite to be rougher. In addition, PVA/CS/HAp nanofibers became more hydrophilic after oxygen gas vacuum plasma treatment. The contact angle had an average value of (39.0 ± 0.0005)° before treatment and decreased to (10.3 ± 0.0005)° after oxygen gas vacuum plasma treatment.

Acknowledgment

This research was supported by PNBP funds in 2021 from the Universitas Negeri Malang to HT.

References

[1] E. Sarigol-Calamak and C. Hascicek, "Tissue scaffolds as a local drug delivery system for bone regeneration," in *Cutting-Edge Enabling Technologies for Regenerative Medicine*, H. J. Chun, C. H. Park, I. K. Kwon, and G. Khang, Eds., Singapore: Springer Singapore, 2018, ch. 25, pp. 475–493, doi: 10.1007/978-981-13-0950-2_25.

[2] M. V. Shaik and S. Gangapatnam, "Preparation and in vitro characterization of hydroxyapatite scaffold for bone tissue engineering using bone marrow Mesenchymal cells," *Sci. Spectr.*, vol. 1, no. 4, pp. 439–444, Oct. 2016.

[3] S. Naahidi *et al.*, "Biocompatibility of hydrogel-based scaffolds for tissue engineering applications," *Biotechnol. Adv.*, vol. 35, no. 5, pp. 530–544, Sep. 2017, doi: 10.1016/j.biotechadv.2017.05.006.

[4] S. Kargozar *et al.*, "Hydroxyapatite nanoparticles for improved cancer theranostics," *J. Funct. Biomater.*, vol. 13, no. 3, p. 100, Jul. 2022, doi: 10.3390/jfb13030100.

[5] P. Hui, S. L. Meena, G. Singh, R. D. Agarawal, and S. Prakash, "Synthesis of hydroxyapatite bio-ceramic powder by hydrothermal method," *J. Miner. Mater. Charact. Eng.*, vol. 9, no. 8, pp. 683–692, Aug. 2010, doi: 10.4236/jmmce.2010.98049.

[6] P. Kamalanathan *et al.*, "Synthesis and sintering of hydroxyapatite derived from eggshells as a calcium precursor," *Ceram. Int.*, vol. 40, no. 10, pp. 16349–16359, Dec. 2014, doi: 10.1016/j.ceramint.2014.07.074.

[7] A. Farooq *et al.*, "Synthesis of piroxicam loaded novel electrospun biodegradable nanocomposite scaffolds for periodontal regeneration," *Mater. Sci. Eng.: C*, vol. 56, pp. 104–113, Nov. 2015, doi: 10.1016/j.msec.2015.06.006.

[8] H. Yang, S. Masse, H. Zhang, C. Hélary, L. Li, and T. Coradin, "Surface reactivity of hydroxyapatite nanocoatings deposited on iron oxide magnetic spheres toward toxic metals," *J. Colloid Interface Sci.*, vol. 417, pp. 1–8, Mar. 2014, doi: 10.1016/j.jcis.2013.11.031.

[9] C. P. Dhanalakshmi, L. Vijayalakshmi, and V. Narayanan, "Synthesis and preliminary characterization of polyethylene glycol (PEG)/hydroxyapatite (HAp) nanocomposite for biomedical applications," *Int. J. Phys. Sci.*, vol. 7, no. 13, pp. 2093–2101, Mar. 2012, doi: 10.5897/IJPS11.1495.

[10] F. Mohandes and M. J. R. A. Salavati-Niasari, "Freeze-drying synthesis, characterization and in vitro bioactivity of chitosan/graphene oxide/hydroxyapatite nanocomposite," *RSC Adv.*, vol. 4, no. 49, pp. 25993–26001, May 2014, doi: 10.1039/C4RA03534H.

[11] G. Sargazi, D. Afzali, A. Mostafavi, and S. Y. Ebrahimipour, "Synthesis of CS/PVA biodegradable composite nanofibers as a microporous material with well controllable procedure through electrospinning," *J. Polym. Environ.*, vol. 26, no. 5, pp. 1804–1817, May 2018, doi: 10.1007/s10924-017-1080-8.

[12] S. Franz, S. Rammelt, D. Scharnweber, and J. C. Simon, "Immune responses to implants–a review of the implications for the design of immunomodulatory biomaterials," *Biomater.*, vol. 32, no. 28, pp. 6692–6709, Oct. 2011, doi: 10.1016/j.biomaterials.2011.05.078.

[13] C. R. Arciola, D. Campoccia, and L. Montanaro, "Implant infections: adhesion, biofilm formation and immune evasion," *Nature Rev. Microbiol.*, vol. 16, no. 7, pp. 397–409, Jul. 2018, doi: 10.1038/s41579-018-0019-y.

[14] H. C. Barshilia and N. Gupta, "Superhydrophobic polytetrafluoroethylene surfaces with leaf-like micro-protrusions through Ar+ O2 plasma etching process," *Vacuum*, vol. 99, pp. 42–48, Jan. 2014, doi: 10.1016/j.vacuum.2013.04.020.

[15] P. Das *et al.*, "Surface modification of electrospun PVA/chitosan nanofibers by dielectric barrier discharge plasma at atmospheric pressure and studies of their mechanical properties and biocompatibility," *Int. J. Biol. Macromol.*, vol. 114, pp. 1026–1032, Jul. 2018, doi: 10.1016/j.ijbiomac.2018.03.115.

[16] C. Drouet, "Apatite formation: Why it may not work as planned, and how to conclusively identify apatite compounds," *Biomed. Res. Int.*, vol. 2013, p. 490946, doi: 10.1155/2013/490946.

[17] A. Nur, A. Rahmawati, N. I. Ilmi, S. Affandi, and A. Widjaja, "Electrochemical synthesis of nanosized hydroxyapatite by pulsed direct current method," in *AIP Conf. Proc.*, vol. 1586, no. 1, Feb. 2014, pp. 86–91, doi: 10.1063/1.4866736.

[18] A. Tiwari and M. Bose, "Morphological analysis of nanoparticle agglomerates generated using DEM simulation," *Part. Sci. Technol.*, vol. 40, no. 3, pp. 373–381, 2022, doi: 10.1080/02726351.2021.1973162.

[19] F. Y. Syafaat and Y. Yusuf, "Influence of Ca/P concentration on hydroxyapatite (HAp) from Asian moon scallop shell (Amusium pleuronectes)," *Int. J. Nanoelectron. Mater.*, vol. 12, no. 3, pp. 357–362, Jul. 2019.

[20] Y. Su, K. Li, X. Zhu, C. Wang, and Y. Zhang, "Microwave-hydrothermal method post-treatment of sprayed Ca-P coating," *Ceram. Int.*, vol. 45, no. 1, pp. 874–884, Jan. 2019, doi: 10.1016/j.ceramint.2018.09.258.

[21] E. F. D. Reis *et al.*, "Synthesis and characterization of poly (vinyl alcohol) hydrogels and hybrids for rMPB70 protein adsorption," *Mater. Res.*, vol. 9, pp. 185–191, Jun. 2006, doi: 10.1590/S1516-14392006000200014.

[22] A. Vashist, A. Vashist, Y. K. Gupta, and S. Ahmad, "Recent advances in hydrogel based drug delivery systems for the human body," *J. Mater. Chem. B*, vol. 2, no. 2, pp. 147–166, Jan. 2014, doi: 10.1039/C3TB21016B.

[23] A. G. Sanchez *et al.*, "Chitosan-hydroxyapatite nanocomposites: Effect of interfacial layer on mechanical and dielectric properties," *Mater. Chem. Phys.*, vol. 217, pp. 151–159, Sep. 2018, doi: 10.1016/j.matchemphys.2018.06.062.

[24] L. Berzina-Cimdina and N. Borodajenko, "Research of calcium phosphates using Fourier transform infrared spectroscopy," in *Infrared Spectroscopy: Materials Science, Engineering And Technology*, T. Theopanides, Ed., Reijeka, Croatia: InTech, 2012, ch. 6, pp. 123–148.

[25] M. Ebrahimi, M.G. Botelho, and S. V. Dorozhkin, "Biphasic calcium phosphates bioceramics (HA/TCP): Concept, physicochemical properties and the impact of standardization of study protocols in biomaterials research," *Mater. Sci. Eng.: C*, vol. 71, pp. 1293–1312, Feb. 2017, doi: 10.1016/j.msec.2016.11.039.

[26] R. R. Kumar and M. Wang, "Growth of brushite crystals in sodium silicate gel and their characterization," *Key Eng. Mater.*, vol. 192–195, pp. 19–22, Jul. 2001, doi: 10.4028/www.scientific.net/KEM.192-195.19.

[27] V. B. Suryawanshi and R. T. Chaudhari, "Spectroscopic studies of gel grown zinc doped calcium hydrogen phosphate dihydrate crystals," in *AIP Conf. Proc.*, vol. 1953, no. 1, May 2018, p. 070025, doi: 10.1063/1.5032803.

[28] N. Bano, S. S. Jikan, H. Basri, S. Adzila, and N. Shuaib, "Fabrication and characterization of nanocrystalline hydroxyapatite extracted from bovine bone at different calcination temperatures," *Int. J. Integr. Eng.*, vol. 11, no. 6, pp. 38–44, Sept. 2019, doi: 10.30880/ijie.2019.11.06.005.

[29] Hartatiek, Yudyanto, S. D. Ratnasari, R. Y. Windari, and N. Hidayat, "Solid state reaction synthesis of Si-HA as potential biomedical material: An endeavor to enhance the added value of Indonesian mineral resources," in *IOP Conf. Ser.: Mater. Sci. Eng.*, vol. 202, no. 1, May, 2017, p. 012021, doi: 10.1088/1757-899X/202/1/012021.

[30] I. Garcia-Orue *et al.*, "Novel nanofibrous dressings containing rhEGF and Aloe vera for wound healing applications," *Int. J. Pharm.*, vol. 523, no. 2, pp. 556–566, May 2017, doi: 10.1016/j.ijpharm.2016.11.006.

[31] K. Terpiłowski, A. E. Wiącek, and M. Jurak, "Influence of nitrogen plasma treatment on the wettability of polyetheretherketone and deposited chitosan layers," *Adv. Polym. Technol.*, vol. 37, no. 6, pp. 1557–1569, Oct. 2018, doi: 10.1002/adv.21813.

[32] P. Sundriyal, M. Pandey, and S. Bhattacharya, "Plasma-assisted surface alteration of industrial polymers for improved adhesive bonding," *Int. J. Adhes. Adhes.*, vol. 101, p. 102626, Sep. 2020, doi: 10.1016/j.ijadhadh.2020.102626.